Geochemistry Geophysics Geosystems G3
AN ELECTRONIC JOURNAL OF THE EARTH SCIENCES
Published by AGU and the Geochemical Society

Article
Volume 4, Number 10
8 October 2003
1085, doi:10.1029/2003GC000505
ISSN: 1525-2027

Crustal motion in the Southern Andes (26°–36°S): Do the Andes behave like a microplate?

Benjamin A. Brooks and Michael Bevis
School of Ocean and Earth Science and Technology, University of Hawaii, 1680 East-West Road, Honolulu, Hawaii 96822, USA (bbrooks@soest.hawaii.edu; bevis@hawaii.edu)

Robert Smalley Jr.
Center for Earthquake Research and Information, University of Memphis, 3876 Central Ave Ste 1, Memphis, Tennessee 38152, USA (smalley@ceri.memphis.edu)

Eric Kendrick
School of Ocean and Earth Science and Technology, University of Hawaii, 1680 East-West Road, Honolulu, Hawaii 96822, USA (kendrick@soest.hawaii.edu)

René Manceda
RepsolYPF, 1330 Lake Robbins Drive, The Woodlands, Texas 77380, USA (RMANCEDA@repsolypf.com)

Eduardo Lauría
Instituto Geográfico Militar Argentina, Cabildo 381, Buenos Aires, Argentina (divgeod@mapas.igm.gov.ar)

Rodrigo Maturana
Instituto Geográfico Militar Chile, Dieciocho N° 369, Santiago, Chile (rmaturana@igm.cl)

Mario Araujo
Instituto Nacional de Prevención Sísmica, Roger Balet Norte 47, 5400, San Juan, Argentina (maraujo@inpres.gov.ar)

[1] A new Global Positioning System (GPS)-derived velocity field for the Andes mountains (26°–36°S) allows analysis of instantaneous partitioning between elastic and anelastic deformation at the orogen's opposing sides. Adding an "Andes" microplate to the traditional description of Nazca-South America plate convergence provides the kinematic framework for nearly complete explanation of the observed velocity field. The results suggest the oceanic Nazca boundary is fully locked while the continental backarc boundary creeps continuously at ~4.5 mm/yr. The excellent fit of model to data (1.7 mm/yr RMS velocity misfit), and the relative aseismicity of the upper crust in the interior Andean region in comparison with its boundaries, supports the notion that the mountains are not currently accruing significant permanent strains. Additionally, the model implies permanent deformation is not accumulating throughout the backarc contractional wedge, but rather that the deformation is accommodated only within a narrow deformational zone in the backarc.

Components: 5915 words, 7 figures, 2 tables.

Keywords: Continental deformation; Andes; GPS; interseismic.

Index Terms: 8102 Tectonophysics: Continental contractional orogenic belts; 7230 Seismology: Seismicity and seismotectonics; 8107 Tectonophysics: Continental neotectonics.

Received 2 January 2003; **Revised** 31 March 2003; **Accepted** 23 May 2003; **Published** 8 October 2003.

Brooks, B. A., M. Bevis, R. Smalley Jr., E. Kendrick, R. Manceda, E. Lauría, R. Maturana, and M. Araujo, Crustal motion in the Southern Andes (26°–36°S): Do the Andes behave like a microplate?, *Geochem. Geophys. Geosyst.*, *4*(10), 1085, doi:10.1029/2003GC000505, 2003.

1. Introduction

[2] Surface velocity fields measured with GPS (Global Positioning System) geodesy promise new insight into the incremental processes that actively deform continents and, over geologic time, construct mountains. For continental regions associated with plate boundaries such as the Andes of South America, an interpretive challenge in relating the GPS-derived velocity field to the long-term deformational pattern is that the current pattern likely represents the superposition of an ephemeral (self-reversing) elastic signal driven by the plate boundary earthquake cycle and steadily accumulating deformation that produces mountain growth. Specifically accounting for these two signals is important if we wish to be able to address first order issues such as the degree of seismic coupling at the main plate boundary [*Savage*, 1983] and whether specific instances of continental deformation are more aptly described by the relative motions of rigid microplates or as the deformation of a viscous continuum [*England and McKenzie*, 1982; *Thatcher*, 1995]. Here, we present a new GPS-derived velocity field from a >1000 km long section of the Andes mountains (26–36°S) (Figure 1, Table 1, Table 2). In our analysis, we test the hypothesis that the orogen itself behaves as a rigid unit with a class of models that combines ephemeral (plate boundary) and permanent (microplate) deformational components.

[3] In the Andes, subduction of the oceanic Nazca plate and locking of the subduction interface strains the upper plate until rupture during major earthquakes [*Barazangi and Isacks*, 1976]. Shortening in backarc contractional orogenic wedges such as the Argentine Precordillera (PC) accommodates underthrusting of the South American craton and makes a significant contribution to permanent orogenic deformation [*Allmendinger et al.*, 1990; *Kley and Monaldi*, 1998; *Ramos et al.*, 1996]. *Norabuena et al.* [1998] explained their GPS velocity field for the central Andes (12°–22°S) by assuming the Nazca boundary is only ~ 50% locked and that slip of ~10–15mm/yr occurs on backarc reverse faults locked to 20km depth. *Kendrick et al.* [2001] produced an improved velocity field for the region, and *Bevis et al.* [2001] argued that this favored 100% locking of the Nazca plate boundary and reduced rates of backarc shortening. Similarly, *Klotz et al.* [2001] concluded that the Nazca plate boundary was fully locked, though their analysis did not explicitly include any velocity component from backarc contraction.

[4] Less attention has been focused on interpreting and modeling the velocity field in the backarc region of the Andes, largely because horizontal velocities in these regions tend to be 10 mm/yr or less. In one recent study, however, *Lamb* [2000] found that velocity gradients (from geologic and *Norabuena et al.*'s [1998] GPS data) do not share the same orientation as calculated buoyancy stress gradients in the central Andean foreland; thus, the thin viscous sheet approximation has not been applied to this portion of the Andes as successfully as it has been

Figure 1. (opposite) GPS velocity field superimposed on Andean topography. Inset shows map of South America with the study area highlighted (red box) and stations used to define the reference frame (blue circles). Plates denoted with magenta labels. White contours are of the subducted Nazca plate and red triangles denote schematically the presence of active arc volcanism [*Cahill and Isacks*, 1992]. Yellow tic mark is the Nazca-South America convergence direction with a magnitude of ~63 mm/yr.

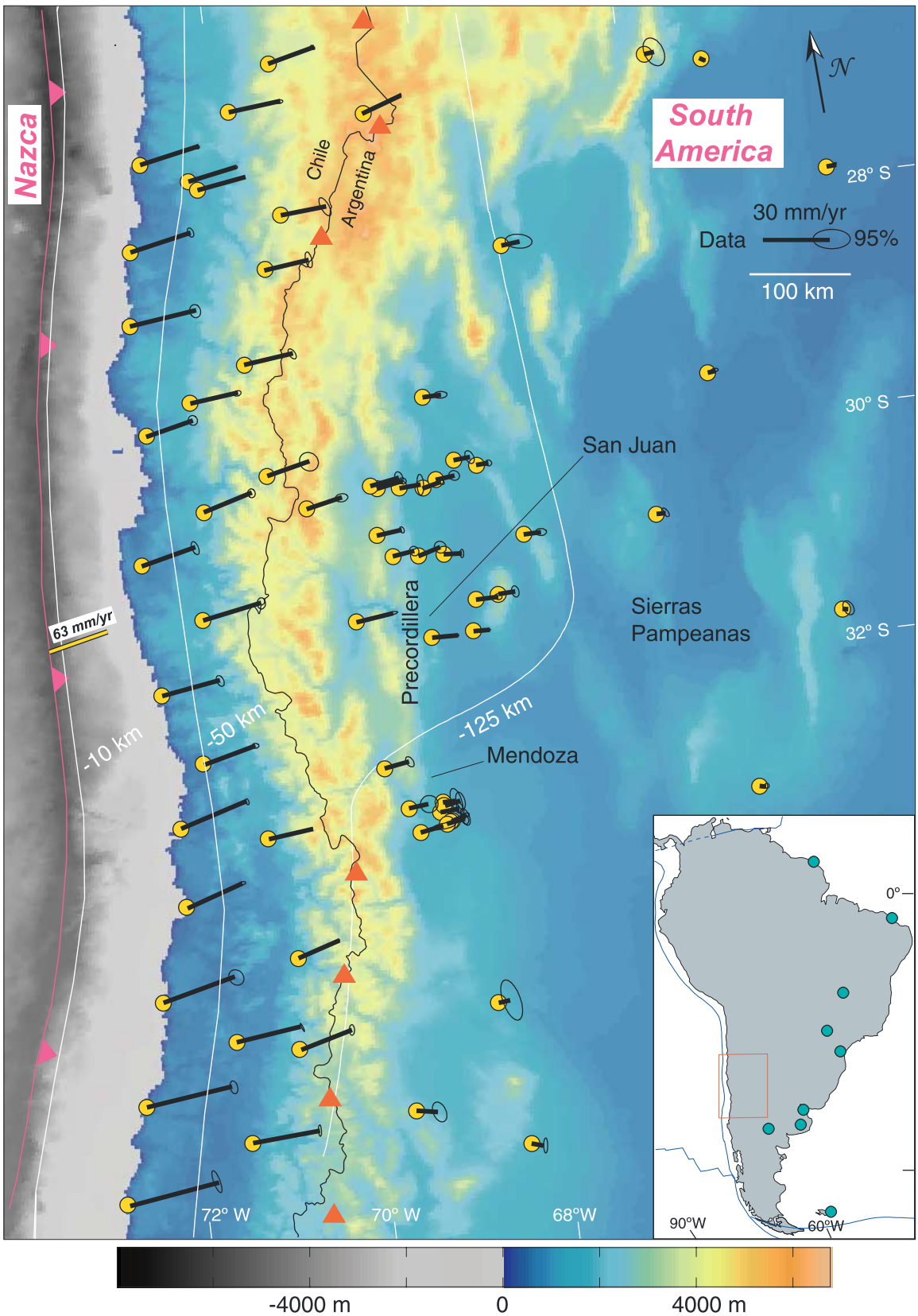
Nazca
South America
Chile
Argentina
N
28° S
30 mm/yr
Data
95%
100 km
30° S
San Juan
Precordillera
Sierras
Pampeanas
32° S
63 mm/yr
-10 km
-50 km
-125 km
Mendoza
0°
72° W
70° W
68°W
90°W
60°W
-4000 m
0
4000 m

Table 1. GPS Site Velocity[a]

Code	Lat	Long	Tspan	Vn	SigVn	Ve	SigVe	CorNE
ACOL	−30.7834	−66.2134	7.25	0.43	0.77	4.00	0.68	−0.64
AT03	−30.8935	−68.4264	3.37	0.39	0.73	7.91	0.34	−0.14
AT05	−30.8483	−68.9495	3.29	2.43	0.85	9.47	0.83	−0.16
AT06	−30.8787	−68.6879	3.40	3.97	1.06	9.57	1.06	−0.12
AT10	−30.2893	−68.5464	3.39	2.94	0.51	8.13	0.57	−0.47
AT12	−30.2332	−68.4026	3.40	2.04	0.87	8.16	0.95	−0.11
AT17	−30.0813	−68.1954	3.38	1.39	1.13	7.16	0.85	−0.43
AT20	−30.2610	−68.7820	3.32	1.70	1.86	9.29	0.60	−0.18
AT23	−30.2346	−69.0057	3.31	3.48	0.55	11.21	0.65	−0.15
AT24	−30.2039	−69.0711	3.53	3.67	1.06	12.48	0.75	−0.33
AT25	−30.6447	−69.0763	3.32	2.56	0.55	10.93	0.42	−0.33
AT29	−30.8156	−67.5906	3.27	1.02	0.61	7.68	1.00	0.00
AT30	−30.1523	−67.9716	3.33	0.93	0.52	5.42	0.57	−0.08
AT31	−33.0743	−69.1556	2.99	2.02	1.52	8.46	1.57	0.01
AT32	−33.3004	−69.0728	2.93	2.96	0.65	9.95	2.07	0.59
AT33	−33.1475	−68.8355	3.01	1.74	1.01	8.30	0.64	−0.46
AT35	−33.0619	−68.7961	2.99	0.66	2.20	5.60	1.14	−0.52
AT37	−33.0956	−68.7871	3.04	2.29	1.51	6.81	0.85	−0.42
AT39	−33.2380	−68.7213	2.98	1.77	1.48	5.54	0.88	−0.53
AT40	−33.2408	−68.7387	2.99	2.88	0.38	6.30	0.55	0.11
AT41	−33.2561	−68.7861	3.01	2.18	0.92	7.92	0.66	−0.31
BDSD	−31.6088	−68.6662	4.99	1.15	0.19	11.23	0.21	−0.36
CALD	−27.0827	−70.8621	6.57	8.42	0.35	25.71	0.35	−0.13
CBQA	−36.1383	−72.8018	4.07	10.32	1.95	38.75	0.91	−0.75
CFAG	−31.6022	−68.2326	5.33	0.62	0.05	7.14	0.05	−0.25
CHAM	−27.2976	−70.4142	4.98	6.63	0.21	20.94	0.19	−0.47
CHIG	−31.7530	−71.5198	4.05	7.04	0.95	25.24	0.72	−0.42
CNGT	−31.3744	−69.4162	3.97	3.92	0.28	16.09	0.80	0.55
CNST	−35.3180	−72.4148	4.10	9.26	1.14	37.18	0.71	−0.27
COGO	−31.1534	−70.9753	3.78	7.91	1.00	25.43	0.74	−0.03
CONA	−28.9754	−70.1502	3.77	5.11	0.89	21.27	0.74	−0.54
COPO	−27.3845	−70.3382	4.67	5.92	0.06	20.91	0.05	−0.32
CORR	−36.1540	−68.3546	4.69	−0.97	1.34	5.33	0.36	−0.04
CPDR	−29.6011	−65.5278	7.30	0.85	0.33	3.27	0.64	0.24
GNDL	−29.4935	−68.4188	3.98	1.20	0.60	8.12	1.17	0.07
GRDA	−27.7157	−69.5584	3.75	3.98	1.61	19.80	1.08	−0.68
GYCN	−34.8831	−71.3451	4.07	6.84	0.69	28.00	0.38	−0.92
HUAS	−28.4785	−71.2223	3.77	7.20	1.16	28.87	0.98	−0.13
INCA	−26.7459	−69.9128	3.75	5.09	0.34	22.49	0.74	0.14
JUNT	−29.9791	−70.0939	3.78	6.52	1.66	18.37	1.69	−0.11
LOBO	−34.4316	−72.0468	4.09	11.53	1.37	31.17	1.35	−0.16
MALR	−35.7268	−69.5425	4.07	−0.47	1.76	9.33	1.29	−0.37
MGCR	−31.3088	−67.9268	3.52	1.16	1.00	7.36	0.68	−0.24
MORA	−30.2082	−70.7897	3.78	8.69	0.78	20.94	0.67	−0.10
MORR	−33.2689	−65.4767	7.27	−0.29	0.44	2.86	0.41	−0.05
MROC	−32.9409	−71.5540	4.06	12.28	0.54	28.55	0.33	−0.50
NIHL	−34.8864	−68.5030	4.06	1.26	3.58	5.05	1.94	−0.54
PAGN	−30.3228	−69.7499	7.90	5.24	0.73	15.43	1.12	0.13
PALO	−31.3306	−68.1651	5.47	1.36	0.54	9.80	0.66	−0.05
POBR	−30.5910	−71.5037	3.82	8.42	1.16	23.34	0.72	−0.53
POTR	−26.3744	−69.4581	3.75	7.52	0.39	20.18	0.38	−0.46
PSNF	−26.9319	−68.5988	3.75	8.05	0.37	16.85	0.10	−0.19
PSTO	−28.1716	−69.7938	3.76	4.61	1.40	19.42	0.65	−0.50
QNTA	−31.7966	−64.4273	7.24	−0.07	1.24	2.62	1.02	−0.37
QPOB	−32.4061	−71.2126	6.76	8.32	0.42	22.48	0.62	−0.06
RARI	−35.7868	−71.3472	4.07	5.53	1.00	29.17	0.28	−0.28
RBLS	−27.9118	−64.1192	4.98	0.74	0.17	4.31	0.24	−0.06
RSTD	−33.6335	−71.6350	4.08	10.93	0.31	23.94	0.58	0.31
SANT	−33.1503	−70.6686	8.18	4.57	0.08	19.31	0.05	−0.33
SIFO	−34.2367	−70.5474	4.05	7.74	0.28	17.66	0.10	−0.52
SILA	−29.2404	−70.7496	3.77	4.95	0.48	20.87	0.65	0.19

Table 1. (continued)

Code	Lat	Long	Tspan	Vn	SigVn	Ve	SigVe	CorNE
TAFI	−26.7444	−65.7810	5.50	1.10	2.46	4.33	1.94	−0.36
TENO	−35.0343	−70.6895	4.09	8.70	0.94	22.15	0.46	−0.08
TINO	−28.2602	−67.4245	3.98	1.92	1.25	7.97	2.40	−0.09
TOFO	−29.4594	−71.2384	3.78	7.27	0.87	20.47	0.83	−0.09
TOTO	−27.8324	−71.0961	3.76	8.77	0.82	26.20	0.59	−0.44
TUCU	−26.8433	−65.2304	5.26	−1.24	0.06	2.68	0.07	−0.25
UPSA	−32.6929	−69.3488	7.43	3.04	0.91	10.74	0.76	−0.46

[a] GPS site velocity is expressed relative to the stable South American plate. Code, station code; Lat, latitude; Long, longitude; Tspan, time span of measurements in years; Vn, north component of velocity (mm/yr), SigVn, standard error (mm/yr); Ve, east component of velocity (mm/yr); SigVe, standard error (mm/yr), CorNE, north-east correlation.

applied to, for example, the Tibetan plateau [*England and Molnar*, 1997].

[5] Our study area, between 26°S and 36°S (Figure 1), was chosen so that surface velocity would not be affected by postseismic signals from either the 1995 Antofagasta earthquake to the north [*Klotz et al.*, 1999] or the great 1960 Chile earthquake to the south [*Plafker and Savage*, 1970]. The region is also of interest because the subducted Nazca slab undergoes a pronounced change in dip with which the basement uplifts of the Sierras Pampeanas range coincide [*Jordan et al.*, 1983] (Figure 1).

[6] We installed the network of survey (SGPS) and continuous (CGPS) GPS stations presented here between 1993 and 1997. SGPS measurements were carried out from 1993 to 2001 in sessions of at least 40 hours over consecutive days. Our field, processing, and velocity analysis methods have been described elsewhere [*Bevis et al.*, 1997, 2001; *Kendrick et al.*, 2001]. We realize a craton-fixed frame nominally attached to stable South America (Figure 1, inset) with an RMS residual velocity of 1.0 mm/yr. In this reference frame, Andean velocities are directed eastward toward the craton (Figure 1). Velocities are largest (∼35 mm/yr) closer to the Nazca boundary and decline toward the craton with no obvious evidence of strike-slip deformation [*Siame et al.*, 1997]. Backarc velocity vectors tend to be rotated clockwise with respect to forearc vectors, a pattern similar to that of the south central Andes [*Bevis et al.*, 2001]. Notably, the velocity field shows no obvious or abrupt change in character associated with the changing dip of the subducted Nazca plate (Figure 1).

2. Analysis

[7] We analyze the data in a way that simultaneously addresses both the short-term ephemeral deformation related to the earthquake cycle at the Nazca plate boundary and the residual deformation field that leads to backarc contraction and long-term mountain growth. Although we recognize the utility of continuum models based on a thin viscous sheet in examining long-term Andean evolution [*Lamb*, 2000; *Wdowinski et al.*, 1989], these models do not consider explicitly the short-term elastic deformation related to the plate boundary. Thus we choose to base our analysis on a model that

Table 2. Model Parameters[a]

Parameter	Value
L	***1***
ω_{AS} Lat.	***56.5°N***
ω_{AS} Lon.	***113.9°W***
ω_{AS} ω	***0.087°/Myr***
ω_{NS} Lat.	61.1°N,
ω_{NS} Lon.	93.6°W
ω_{NS} ω	0.57°/Myr
Updip extent	10km
Down-dip extent	50km
Poisson's ratio	.25

[a] Parameters used in the modeling. Parameters in bold italics are solved for in the 3-plate model inversion, other parameters are held fixed. *L*, degree of locking on the Nazca boundary; ω_{AS} Lat., AS Euler pole latitude; ω_{AS} Lon., AS Euler pole longitude; ω_{AS} ω, AS Euler pole angular velocity; ω_{NS} Lat., NS Euler pole latitude; ω_{NS} Lon., NS Euler pole longitude; ω_{NS} ω, NS Euler pole angular velocity; *updip extent*, updip extent of the locked Nazca boundary; down-dip extent, down-dip extent of the locked Nazca boundary; Poisson's ratio, poisson's ratio used in the elastic dislocation modeling.

combines elastic half-space deformation due to slip on embedded discontinuities and the steady motion of rigid plates on a spherical earth [*Bevis et al.*, 2001; *McCaffrey*, 2002].

[8] To best reproduce the smoothly curving geometry of the subduction zone in this ~1000 km long stretch of the Andes we implement our calculations using triangular dislocation elements in an elastic half-space [*Bevis et al.*, 2001]. We find that elastic half-space models driven only by convergence at the Nazca boundary significantly underpredict velocity magnitude at all stations from the trench to the backarc (Figure 2, green vectors). This observation, combined with the evidence that the PC fold and thrust belt has accommodated more than 100 km of shortening during the most recent phase of Andean orogeny [*Allmendinger et al.*, 1990; *Jordan et al.*, 1993; *Zapata and Allmendinger*, 1996], suggests that a 2-plate model [*Williams and McCaffrey*, 2001] may be oversimplified, and so we add an independent microplate to the kinematic description of Nazca-South America convergence.

[9] Our preferred analysis employs a 3-plate model in which an Andean microplate (A) is located between the Nazca (N) and South America (S) plates (Figure 3). At timescales large compared with that of the earthquake cycle, relative plate motions are steady and can be described using Euler vectors (ω) [*Cox and Hart*, 1986] subject to the constraint that $\omega_{NS} = \omega_{NA} + \omega_{AS}$. We assume that the A–S boundary creeps continuously at a constant rate on what we envision as a sub-horizontal décollement rooted at deeper crustal levels beneath the Andean arc. The only explicit geometrical assumption we make about the A-plate is that the A–S surface trace is chosen to correspond with the geologically youngest structures of the thrust front (Figure 2). Where station spacing is sparse, the precise location of the surface trace does not affect the model results. We treat locking of the Nazca boundary as an elastic perturbation superimposed on steady plate convergence [*Savage*, 1983]. The magnitude of this perturbation, the elastic loading field, is proportional to the degree of locking, L, at the N–A boundary. The velocity field in A is then a combination of elastic loading and steady A–S plate convergence, whereas in S all motion is due to elastic loading.

[10] Previous workers have attempted to model similar data sets by solving for the lower locking depth on the subduction interface [*Klotz et al.*, 2001] as well as solving for the down-dip and along-strike variations in coupling [*McCaffrey et al.*, 2000]. In preliminary analyses we found that inclusion of these added components to the model did not significantly improve model-data misfit while adding as many as 9 parameters to the inverse problem. Thus by assuming uniform along-strike and down-dip coupling and a lower locking depth of 50km we are able to describe our 3 plate model with only 4 parameters (L and the 3 parameters describing the euler vector, ω_{AS}).

[11] We find the best-fitting velocity model by repeatedly selecting L and ω_{AS}, calculating ω_{NA}, and minimizing misfit with an L_1 norm using a Nelder-Mead simplex algorithm. In order to do this we must adopt a value for ω_{NS}. We [*Kendrick et al.*, 2003] and others [*Angermann et al.*, 1999; *Norabuena et al.*, 1999] have used GPS velocities to find the modern Euler vector describing N–S plate convergence. These studies find convergence velocities significantly slower than the geologically averaged value predicted by the Nuvel −1A plate model [*DeMets et al.*, 1994]; thus, we choose to adopt a modern value as opposed to the other approaches [*Ruegg et al.*, 2002]. We use our estimate for ω_{NS} with a pole at 61.1°N, 93.6°W

Figure 2. (opposite) GPS velocity field with best 3-plate model (red vectors) and 2-plate model (green vectors) superimposed on Andean topography. Magenta lines denote the western and eastern boundaries of the proposed 'Andean' plate, with the hachures on the overthrusting plate (see Figure 3 for a description of the 3-plate model). White triangles are the dislocation elements used in the elastic portion of the model with the upper (−10 km) and lower (−50 km) boundaries constrained by earthquake catalogs [*Cahill and Isacks*, 1992]. Bold black angle marks contain the yellow stations in the velocity profile which is denoted by the black dashed line (Figure 5).A-A' and B-B' are the geologic cross-sections in Figure 7. All other annotation as in Figure 1.

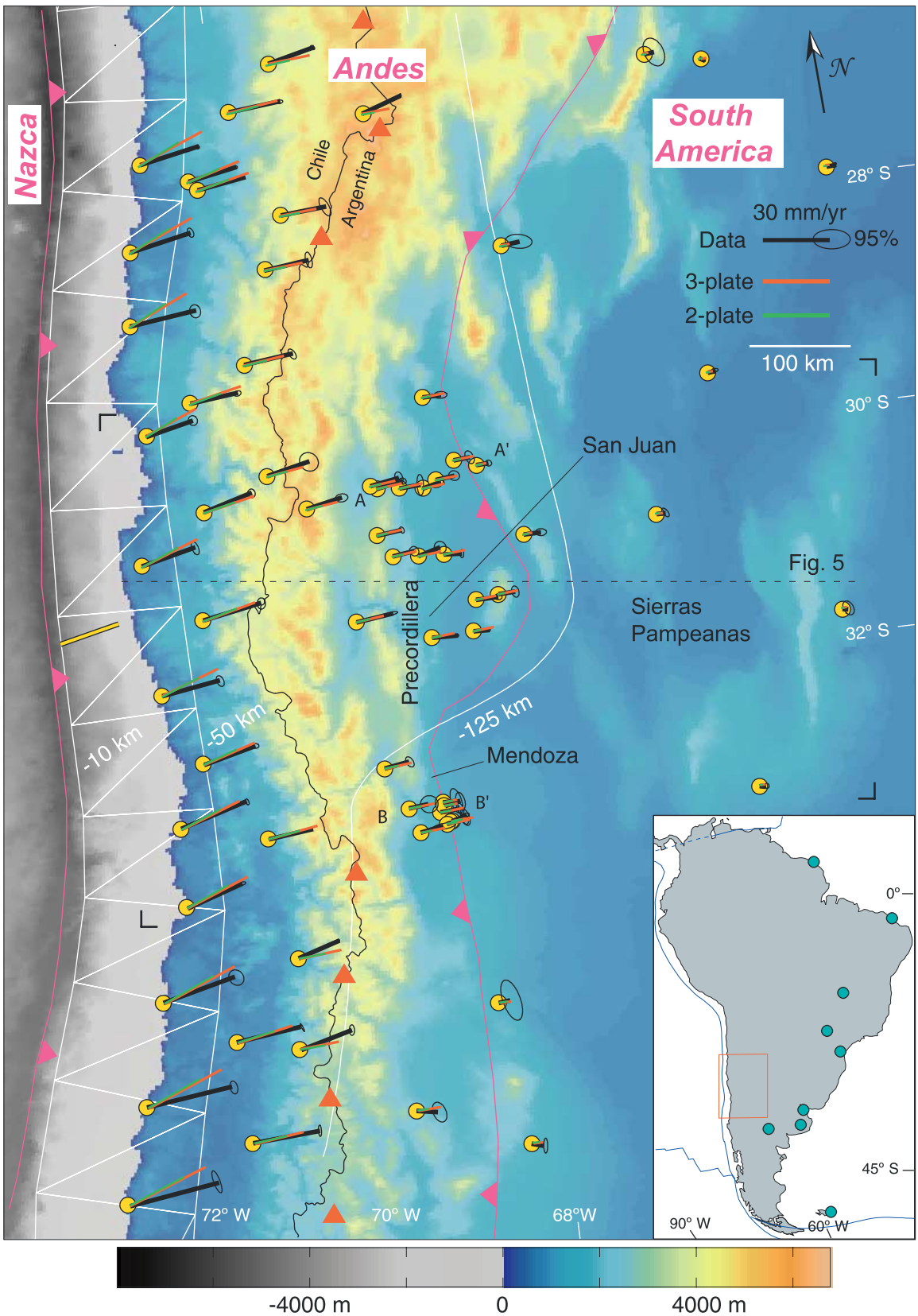
Andes
Nazca
South America
Chile
Argentina
N
28° S
30 mm/yr
Data
95%
3-plate
2-plate
100 km
30° S
San Juan
A
A'
Fig. 5
Precordillera
Sierras Pampeanas
32° S
-10 km
-50 km
-125 km
Mendoza
B
B'
0°
45° S
72° W
70° W
68°W
90° W
60° W
-4000 m
0
4000 m

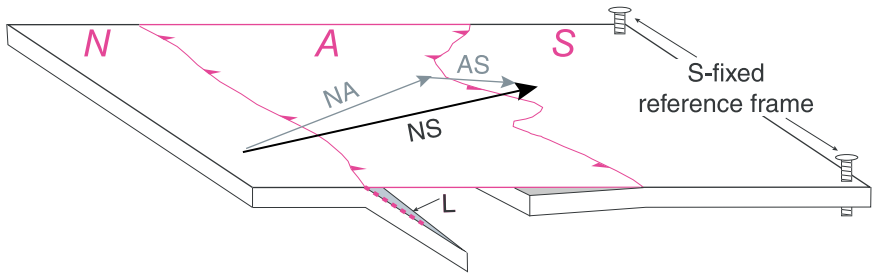

Figure 3. Cartoon of the three plate model in a South America fixed reference frame. Magenta lines and symbols as in Figure 2. Dashed magenta line is the locked portion of the subduction zone with degree of locking, L.

and a rate of 0.57°/Myr. At a latitude of 31°S, N–S plate convergence is ~63 mm/yr and is rotated ~10° anticlockwise from the normal to the Peru-Chile trench (Figure 2).

3. Results and Discussion

[12] The best model, with an RMS velocity misfit of just 1.7 mm/yr (Figure 2), depicts an Andean orogenic system whose boundaries are asymmetrically coupled: the N boundary is 100% locked while the A plate creeps continuously over the S plate with a horizontal velocity of ~4.5 mm/yr. To assess the robustness of our findings, for the range of L values, we ran a series of 100 inversions with independent and randomly chosen starting points (Figure 4). The results clearly illustrate that the RMS misfit of the best-fitting models steadily decreases as L is increased toward full locking (Figure 4).

[13] The elastic loading component (green vectors, Figure 2; blue line, Figure 5) controls the velocity field's cratonward decay and clockwise rotation [*Bevis and Martel*, 2001], and it can be recovered by future seismic or aseismic [*Dragert et al.*, 2001; *Miller et al.*, 2002] slip events at the Peru-Chile trench. This component explains ~70% or more of the velocity magnitude for stations throughout

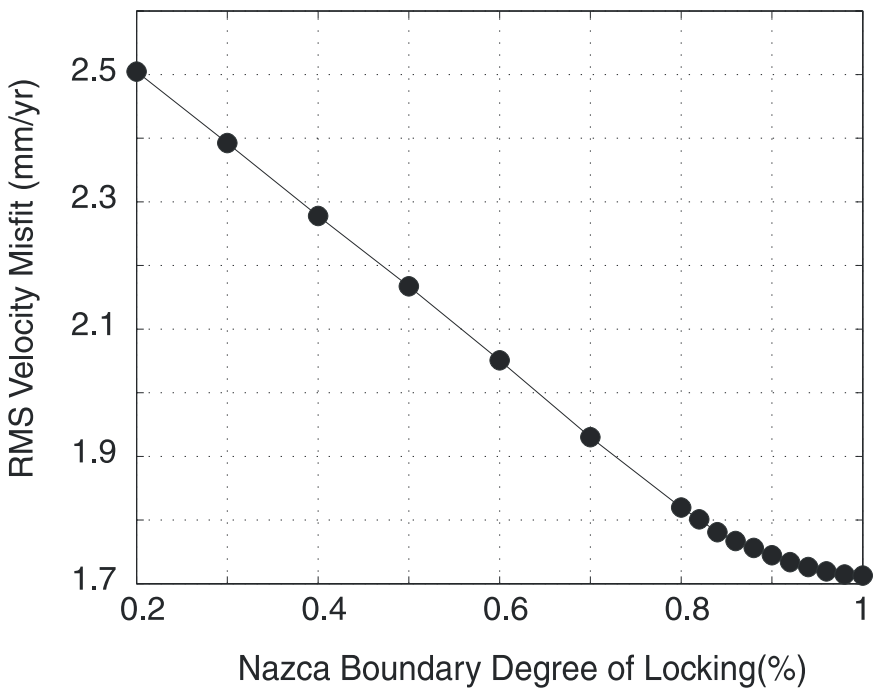

Figure 4. Plot of RMS velocity misfit versus Nazca boundary locking rate. Fully locked = 1. Each data point represents the minimum value from 100 inversions with independent and randomly chosen starting points.

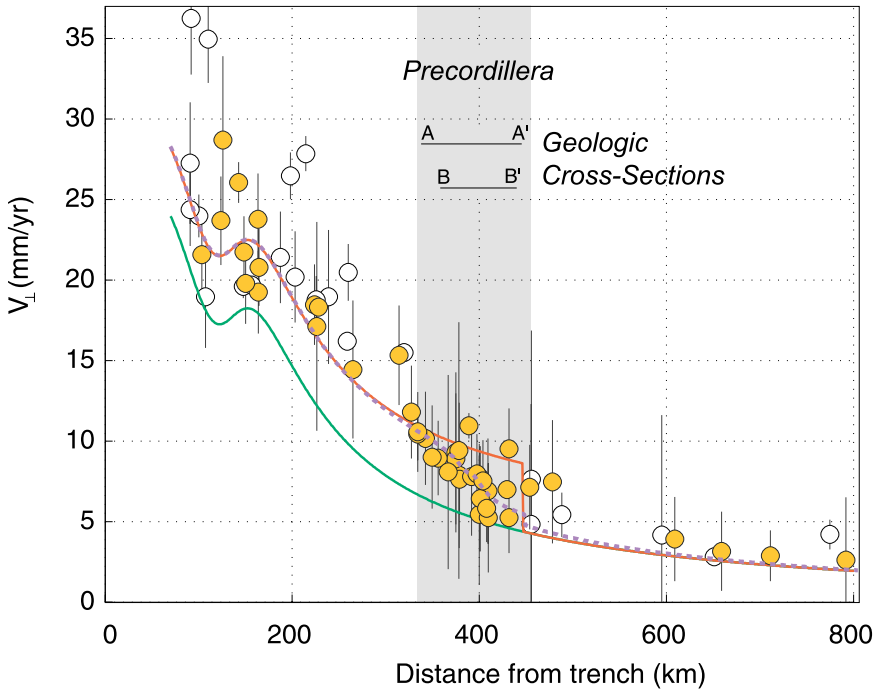

Figure 5. Velocity profile taken along the dashed line in Figure 2 plots trench-normal distance vs. trench-normal velocity, $V_{\perp}$. Yellow circles are stations within the corner marks on Figure 2, white circles are stations outside of the marks. Error bars are 95% confidence. Smooth curves are profiles for the elastic loading component, the best 3-plate model, and the corrected 3-plate model. The green line is the elastic component of the best 3-plate model (red line). The elastic component is equivalent to a "2-plate" model. Dashed magenta line is the corrected best model.

most of the A plate; far from the trench, it accounts for essentially the entire velocity field in the S plate including the seismically active Sierras Pampeanas region [*Costa and Vita-Finzi*, 1996] (Figure 5). The ω_{AS} (56.5°N, 113.9°W, 0.087°/Myr) Euler pole and ω_{NS} are only slightly non-coaxial; thus, A–S convergence is rotated ~10° clockwise from N–S plate convergence. The microplate motion contributes a nearly uniform velocity increase for all stations on the A plate and accounts for the steady state portion of the velocity signal. To the extent that we may compare data sets with temporal scales differing by 6 orders of magnitude, the ~4.5mm/yr magnitude of the steady signal agrees very well with the post ~2.7 Ma shortening rate of ~5mm/yr determined for the structures in the eastern PC [*Zapata and Allmendinger*, 1996].

[14] The excellent agreement between data and model warrants serious consideration of the notion that, at least over the decadal timescale reported here, the Andean region (the "A" plate) does not accrue significant permanent strains and behaves as a "microplate" overthrusting the stable South American craton. In support of this, a plot of epicenters of shallow crustal earthquakes (depth < 30 km) from a nearly complete catalog of earthquakes with $M_w > 5.2$ [*Engdahl et al.*, 1998] is consistent with the idea of a stable, largely aseismic, Andean region accruing permanent strains only at its narrow boundary zones (Figure 6). In apparent contrast to the Andes, the region associated with the India-Asia collision and the Himalayan orogen exhibits a diffuse pattern of seismicity distributed throughout the Tibetan plateau (Figure 6) in a manner more consistent with a continental region deforming as a continuum [*England and Molnar*, 1997]. That the Andean region currently behaves as an independent block whose kinematics can be well-modeled as a microplate, however, does not imply that it has done so consistently during this most recent orogenic phase lasting close to 20 Myrs [*Mpodozis and Ramos*, 1989]. Proper assessment of the longer-term deformational comportment of the interior Andean region will require significantly more high

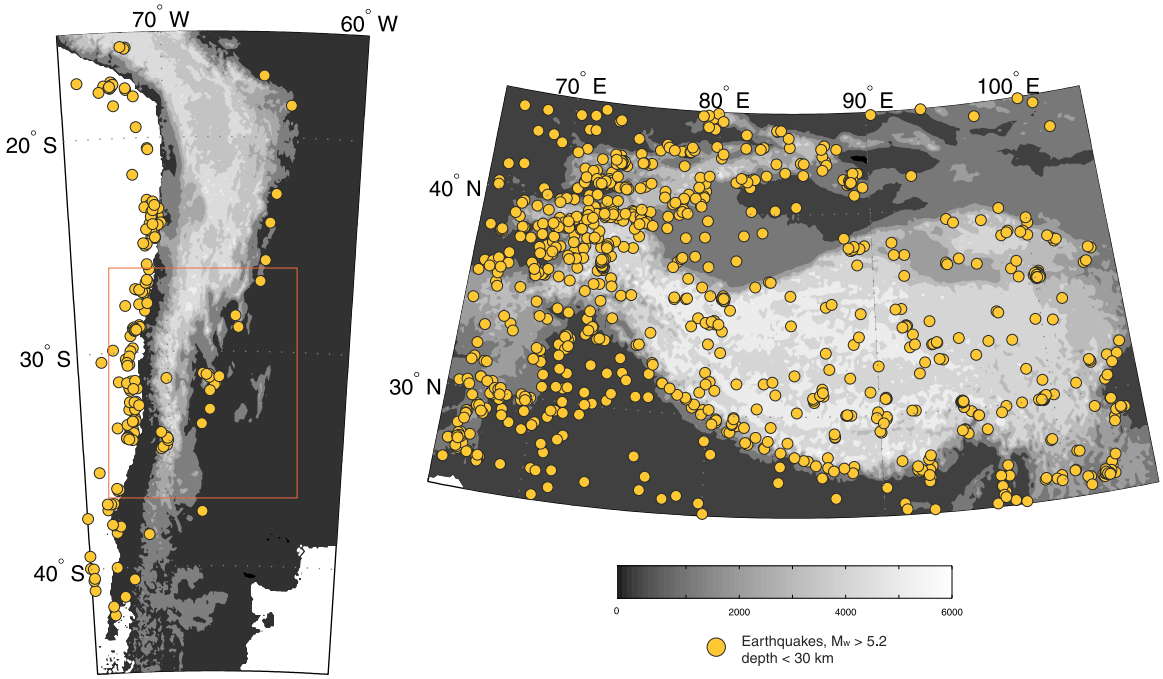

Figure 6. Topography and shallow crustal seismicity (<30 km) from **A**, the Andes and **B**, the Tibetan plateau taken from the catalog of Engdahl [*Engdahl et al.*, 1998].

resolution studies of quaternary faulting throughout the Andes [*Siame et al.*, 2002, 1997].

[15] In the northern- and southern-most sections of the study area, model vectors nearest the trench tend to be rotated slightly to the north of the data vectors, whereas those closest to the volcanic arc tend to be rotated to the south (Figure 2). These regions of poorer conformance to the 3-plate model are spatially correlated with sections of the mountains where the volcanic arc is currently active and subduction is steep, in contrast to the central portion of the study area where there has been no active arc volcanism for the past 6 Ma and subduction is flat [*Isacks*, 1988]. We speculate that the active arc may be associated with a thermally weakened zone that leads to this second-order deviation from the 3-plate model.

[16] Although the velocity data do not require that intracontinental subduction [*Bally and Snelson*, 1980] is the active backarc process (similar data from other active orogenic environments such as New Zealand, for example, are explained differently [*Beavan et al.*, 1999]) the kinematics defined by the 3-plate model is consistent with the notion that intracontinental subduction occurs at the A–S boundary. In support of this, there is substantial evidence from balanced cross-sections from the study area that continental crust has been underthrust beneath the contractional wedge during the past ~20 Ma of Andean orogenesis [*Allmendinger et al.*, 1990; *Ramos et al.*, 1996; *Zapata and Allmendinger*, 1996]. Additionally, further north, seismological data indicate that the Brazilian craton currently underthrusts the Andean region as far west as the Bolivian Eastern

Figure 7. (opposite) Geologic cross-sections and Precordillera velocity field with model and residuals (white vectors) for Figure 7a, the region near San Juan and Figure 7b, the region near Mendoza superimposed on a Land Sat 5 Thematic Mapper mosaic. Symbols as in 1A, error ellipses (95% confidence) referred to residuals. Magenta triangle on cross-sections is location of A-plate boundary. Cross-sections compiled from references in the text and an unpublished section from the Mendoza area. N, Niquivil Anticline; LS, Las Salinas Anticline; B, Bermejo Anticline; LP, La Pilona Anticline; Ba, Barrancas Anticline. In both cross-section and map view the dashed magenta line is the continuously creeping, down-dip extent of the locked zone used as a correction to the preferred model (Figure 5).

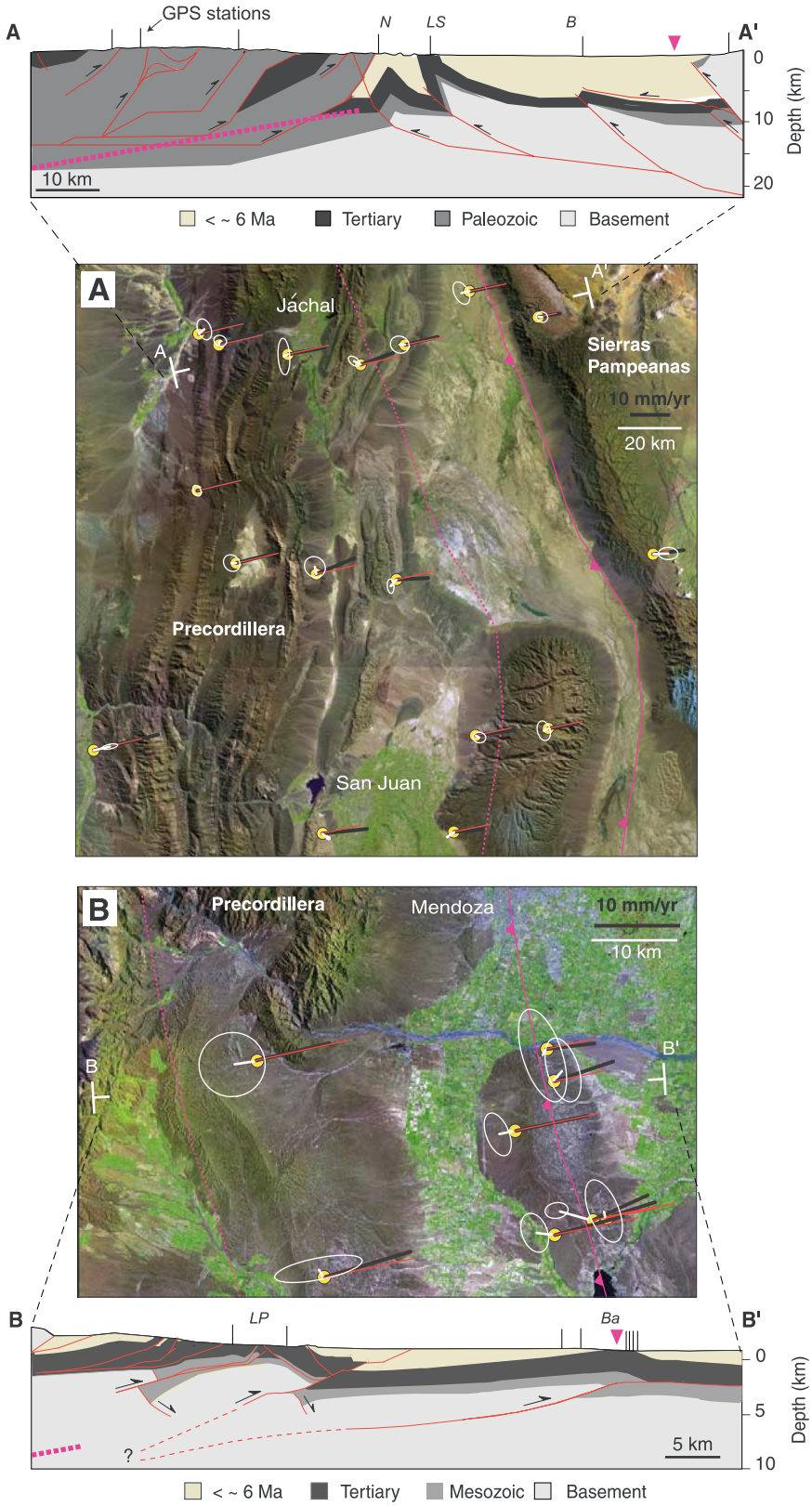
A
GPS stations
N
LS
B
A'
0
10
20
Depth (km)
10 km
< ~ 6 Ma
Tertiary
Paleozoic
Basement
A
Jáchal
A
A'
Sierras
Pampeanas
10 mm/yr
20 km
Precordillera
San Juan
B
Precordillera
Mendoza
10 mm/yr
10 km
B
B'
B
LP
Ba
B'
0
5
10
Depth (km)
?
5 km
< ~ 6 Ma
Tertiary
Mesozoic
Basement

Cordillera [*Beck and Zandt*, 2002]. We do not, however, intend to suggest that intracontinental subduction has progressed to the point that continental material is being subducted into the mantle beneath the Andean arc - a process that may or may not be physically unlikely [*Molnar and Gray*, 1979].

[17] Our analysis places strong constraint on the mechanical behavior of the backarc contractional wedge by demonstrating that permanent deformation is currently accommodated at the front of the PC fold and thrust belt and not distributed throughout its width. This is consistent with the narrow band of seismicity described above (Figure 6) and also with post-20 Ma geological reconstructions demonstrating eastward migration of the PC through active deformation near its tip [*Jordan et al.*, 1993; *Zapata and Allmendinger*, 1996]. In the context of an orogenic wedge whose kinematics are forced by the competition between tectonics and erosion [*Dahlen and Suppe*, 1988], it is also illustrative to consider mountain belt scale geomorphic indices demonstrating that the eastern margin of the Andes between ~17° and 36°S is a regime of relatively low erosional intensity [*Montgomery et al.*, 2001]. The combined geodetic, geologic, and geomorphic analyses suggest that the PC has not attained a steady state balance of erosion and tectonics, but rather, that it continually widens through accretion of new material at its toe.

[18] Our modeling is carried out at the plate tectonic scale and is not intended to be precise at the scale of individual structures. For instance, though the model provides an excellent fit to the data as a whole, residual examination demonstrates a small, but systematic velocity overprediction near the A–S boundary (Figures 2 and 7). The spatial coherence suggests this signal is significant, albeit second-order, even though individual residual vectors are rarely larger than their associated uncertainty. We can account for this anomaly by modifying our model: we assume that the A–S boundary dips westward at 10° and is locked from its tip to a down-dip length of ~50km (Figure 7). (Here, we model backarc locking using the backslip formalism in the same way as at the Nazca boundary.) This simple (and probably non-unique) correction is sufficient throughout the PC despite the fact that the structures comprising the locked zone differ in the north and south [*Brooks et al.*, 2000; *Jordan et al.*, 1993; *Zapata and Allmendinger*, 1996] (Figure 7). In the north, the west-vergent Niquivil, Las Salinas, and Bermejo anticlines comprise the locked zone and the Sierra de Valle Fertil thrust fault, the westernmost expression of the Sierras Pampeanas basement uplifts, abuts the A–S boundary (Figure 7a). In the south, the zone is composed of only two, east-vergent structures, the La Pilona and Barrancas anticlines, and the thrust front is separated from the westernmost expression of the Sierras Pampeanas by ~200 km of undeformed foreland basin strata (Figure 7d). Discerning the details of deformation in the frontal zone, such as activity, strain accumulation, and seismic hazard of individual structures, will require finer velocity resolution through longer measurement time spans.

[19] That we find the décollement below the A-plate to be continuously creeping does not imply that it is "freely" slipping in the sense that it is shear traction-free. On the contrary, we envision this boundary to be viscously coupled, a configuration that allows both continuous motion and stress transmission across the boundary. Thus we speculate that transmission of stresses across the fully locked oceanic subduction boundary drives microplate motion and deformation at the intracontinental boundary. If the stress drop associated with major subduction earthquakes is small compared to the failure stress, then creep at the A–S boundary should vary only slightly during the earthquake deformation cycle at the Nazca boundary.

Acknowledgments

[20] Funding provided by NSF grants EAR-9115576 and EAR-9615393. We thank R. Allmendinger and C. Wolfe for previous reviews of this paper. We especially acknowledge Fernando Galban of IGM Argentina for his continuing support and collaboration. We gratefully acknowledge the many peo-

ple whose collaboration in the field made this project possible. These include but are not limited to: A. A. Garcia, B. Knight, R. Barriga, H. Parra, W. Rubio, P. Gallardo, J. Baron, M. Blanco, P. Euillades, L. Euillades, V. Bonfils, G. Cabrera, C. Gardini, J. Argento, S. Bea, J. Yu, M. Burns, M. Patrick, and F. Forconesi. This is SOEST contribution 6174 and CERI contribution 473.

References

Allmendinger, R., D. Figueroa, D. Snyder, J. Beer, C. Mpodozis, and B. L. Isacks, Foreland shortening and crustal balancing in the Andes at 30°S latitude, *Tectonics*, *9*, 789–809, 1990.

Angermann, D., J. Klotz, and C. Reigber, Space-geodetic estimation of the Nazca-South America Euler vector, *Earth Planet. Sci. Lett.*, *171*, 329–334, 1999.

Bally, A. W., and S. Snelson, Realms of subsidence, in *Facts and Principles of World Oil Occurrence*, vol. 6, edited by A. D. Miall, pp. 9–75, Can. Soc. of Petrol. Geol., Calgory, 1980.

Barazangi, M., and B. Isacks, Spatial distribution of earthquakes and subduction of the Nazca plate beneath South America, *Geology*, *4*, 686–692, 1976.

Beavan, J., et al., Crustal deformation during 1994–1998 due to oblique continental collision in the central Southern Alps, New Zealand, and implications for seismic potential of the Alpine Fault, *J. Geophys. Res.*, *104*, 25,233–25,255, 1999.

Beck, S. L., and G. Zandt, The nature of orogenic crust in the central Andes, *J. Geophys. Res.*, *107*(B10), 2230, doi:10.1029/2000JB000124, 2002.

Bevis, M., and S. Martel, Oblique plate convergence and interseismic strain accumulation, *Geochem. Geophys. Geosyst.*, *2*, Paper number 2000GC000125, 2001.

Bevis, M., Y. Bock, P. Fang, R. Reilinger, T. Herring, J. Stowell, and R. Smalley Jr., Blending old and new approaches to regional geodesy, *Eos Trans. AGU*, *78*, 61, 64–66, 1997.

Bevis, M., E. Kendrick, R. Smalley Jr., B. A. Brooks, R. W. Allmendinger, and B. L. Isacks, On the strength of interplate coupling and the rate of back arc convergence in the central Andes: An analysis of the interseismic velocity field, *Geochem. Geophys. Geosyst.*, *2*, 10.129/2001GC000198, 2001.

Brooks, B. A., E. Sandvol, and A. Ross, Fold style inversion: Placing probabilistic constraints on the predicted shape of blind thrust faults, *J. Geophys. Res.*, *105*, 13,281–13,302, 2000.

Cahill, T., and B. L. Isacks, Seismicity and shape of the subducted Nazca plate, *J. Geophys. Res.*, *97*, 17,503–17,529, 1992.

Costa, C. H., and C. Vita-Finzi, Late Holocene faulting in the southeast Sierras Pampeanas of Argentina, *Geology*, *24*, 1127–1130, 1996.

Cox, A., and R. B. Hart, *Plate Tectonics How it Works*, 392 pp., Blackwell Sci., Cambridge, Mass., 1986.

Dahlen, F. A., and J. Suppe, Mechanics, growth, and erosion of mountain belts, *Spec. Pap. Geol. Soc. Am.*, *218*, 161–178, 1988.

DeMets, C., R. G. Gordon, D. F. Argus, and S. Stein, Effect of recent revisions to the geomagnetic reversal time scale on estimates of current plate motions, *Geophys. Res. Lett.*, *21*, 2191–2194, 1994.

Dragert, H., K. Wang, and T. S. James, A silent slip event on the deeper Cascadia subduction interface, *Science*, *292*, 1525–1528, 2001.

Engdahl, E. R., R. D. van der Hilst, and R. P. Buland, Global teleseismic earthquake relocation with improved travel times and procedures for depth determination, *Bull. Seismol. Soc. Am.*, *88*, 722–743, 1998.

England, P., and D. McKenzie, A thin viscous sheet model for continental deformation, *Geophys. J. R. Astron. Soc.*, *70*, 295–321, 1982.

England, P., and P. Molnar, Active deformation of Asia; from kinematics to dynamics, *Science*, *278*, 647–650, 1997.

Isacks, B. L., Uplift of the Central Andean Plateau and Bending of the Bolivian Orocline, *J. Geophys. Res.*, *93*, 3211–3231, 1988.

Jordan, T. E., B. L. Isacks, R. W. Allmendinger, J. A. Brewer, V. Ramos, and C. J. Ando, Andean tectonics related to geometry of subducted Nazca plate, *Geol. Soc. Am. Bull.*, *94*, 341–361, 1983.

Jordan, T. E., R. W. Allmendinger, J. F. Damanti, and R. E. Drake, Chronology of motion in a complete thrust belt: The Precordillera, 30–31°S, *Andes Mountains, J. Geol.*, *101*, 135–156, 1993.

Kendrick, E., M. G. Bevis, R. Smalley Jr., and B. A. Brooks, An integrated crustal velocity field for the central Andes, *Geochem. Geophys. Geosyst.*, *2*, 10.1029/2001GC000191, 2001.

Kendrick, E., M. Bevis, R. Smalley Jr., B. Brooks, R. B. Vargas, E. Lauría, and L. P. S. Fortes, The Nazca-South America Euler Vector and its Rate of Change, *J. South Am. Earth Sci.*, in press, 2003.

Kley, J., and C. R. Monaldi, Tectonic shortening and crustal thickness in the Central Andes: How good is the correlation, *Geology*, *26*, 723–726, 1998.

Klotz, J., et al., GPS-derived Deformation of the Central Andes Including the 1995 Antofagasta Mw = 8.0 Earthquake, *Pure Appl. Geophys.*, *154*, 709–730, 1999.

Klotz, J., G. Khazaradze, D. Angermann, C. Reigber, R. Perdomo, and O. Cifuentes, Earthquake cycle dominates contemporary crustal deformation in Central and Southern Andes, *Earth Planet. Sci. Lett.*, *193*, 437–446, 2001.

Lamb, S., Active deformation in the Bolivian Andes, South America, *J. Geophys. Res.*, *105*, 25,627–25,653, 2000.

McCaffrey, R., Crustal block rotations and plate coupling, in *Plate Boundary Zones*, *Geodyn. Ser.*, vol. 30, edited by S. Stein and J. T. Freymueller, pp. 101–122, AGU, Washington, D.C., 2002.

McCaffrey, R., M. D. Long, C. Goldfinger, P. C. Zwick, J. L. Nabelek, C. K. Johnson, and C. Smith, Rotation and plate locking at the southern Cascadia subduction zone, *Geophys. Res. Lett.*, *27*, 3117–3120, 2000.

Miller, M. M., T. Melbourne, D. J. Johnson, and W. Q. Sumner, Periodic slow earthquakes from the Cascadia Subduction Zone, *Science*, *295*, 2423, 2002.

Molnar, P., and D. Gray, Subduction of continental lithosphere: Some constraints and uncertainties, *Geology*, *7*, 58–62, 1979.

Montgomery, D. R., G. Balco, and S. D. Willett, Climate, tectonics, and the morphology of the Andes, *Geology*, *29*, 579–582, 2001.

Mpodozis, C., and V. Ramos, The Andes of Chile and Argentina, in *Geology of the Andes and its Relation to Hydrocarbon and Mineral Resources*, *Earth Sci. Ser.*, edited by G. E. Ericksen et al., pp. 59–90, Circum-Pacific Council for Energy and Mineral Resources, Menlo Park, Calif., 1989.

Norabuena, E. O., T. H. Dixon, S. Stein, and C. G. A. Harrison, Decelerating Nazca-South America and Nazca-Pacific plate motions, *Geophys. Res. Lett.*, *26*, 3405–3408, 1999.

Plafker, G., and J. C. Savage, Mechanism of the Chilean earthquake of May 21 and 22, 1960, *Geol. Soc. Am. Bull.*, *81*, 1001–1030, 1970.

Ramos, V. A., M. Cegarra, and E. Cristallini, Cenozoic tectonics of the High Andes of west-central Argentina (30–36° latitude), *Tectonophysics*, *259*, 185–200, 1996.

Ruegg, J. C., J. Campos, R. Madariaga, E. Kausel, J. B. de Chabalier, R. Armijo, D. Dimitriv, I. Georgiev, and S. Barrientos, Interseismic strain accumulation in south central Chile from GPS measurements, 1996–1999, *Geophys. Res. Lett.*, *29*, 1517, 2002.

Savage, J. C., A dislocation model of strain accumulation and release at a subduction zone, *J. Geophys. Res.*, *88*, 4984–4996, 1983.

Siame, L. L., D. L. Bourles, M. Sebrier, O. Bellier, J. C. Castano, M. Araujo, M. Perez, G. M. Raisbeck, and F. Yiou, Cosmogenic dating ranging from 20 to 700 ka of a series of alluvial fan surfaces affected by the El Tigre fault, Argentina, *Geology*, *25*, 975–978, 1997.

Siame, L. L., O. Bellier, M. Sebrier, D. L. Bourles, P. Leturmy, and M. Perez, Seismic hazard reappraisal from combined structural geology, geomorphology and cosmic ray exposure dating analyses: The Eastern Precordillera thrust system (NW Argentina), *Geophys. J. Int.*, *150*, 241–260, 2002.

Thatcher, W. R., Microplate versus continuum descriptions of active tectonic deformation: *J. Geophys. Res.*, *100*, 3885–3894, 1995.

Wdowinski, S., R. J. O'Connell, and P. England, A continuum model of continental deformation above subduction zones; application to the Andes and the Aegean, *J. Geophys. Res.*, *94*, 10,331–10,346, 1989.

Williams, C., and R. McCaffrey, Stress rates in the central Cascadia subduction zone inferred from an elastic plate model, *Geophys. Res. Lett.*, *28*, 2125–2128, 2001.

Zapata, T. R., and R. W. Allmendinger, Growth stratal records of instantaneous and progressive limb rotation in the Precordillera thrust belt and Bermejo basin, Argentina, *Tectonics*, *15*, 1065–1083, 1996.